

## Supporting Information

### A sequential process to synthesize $\text{Fe}_3\text{O}_4@\text{MnO}_2$ hollow nanospheres for high performance supercapacitors

Chengyu Tu<sup>#a</sup>, Xuan Li<sup>#a</sup>, Congcong Lu<sup>a</sup>, Qiao Luo<sup>a</sup>, Tie Li<sup>b\*</sup>, Maiyong Zhu<sup>a\*</sup>

<sup>a</sup> Research School of Polymeric Materials, School of Materials Science & Engineering,

Jiangsu University, Zhenjiang, 212013, P. R. China

<sup>b</sup> i-Lab, Suzhou Institute of Nano-Tech and Nano-Bionics (SINANO), Chinese Academy of  
Sciences (CAS), 398 Ruoshui Road, Suzhou, 215123, P. R. China

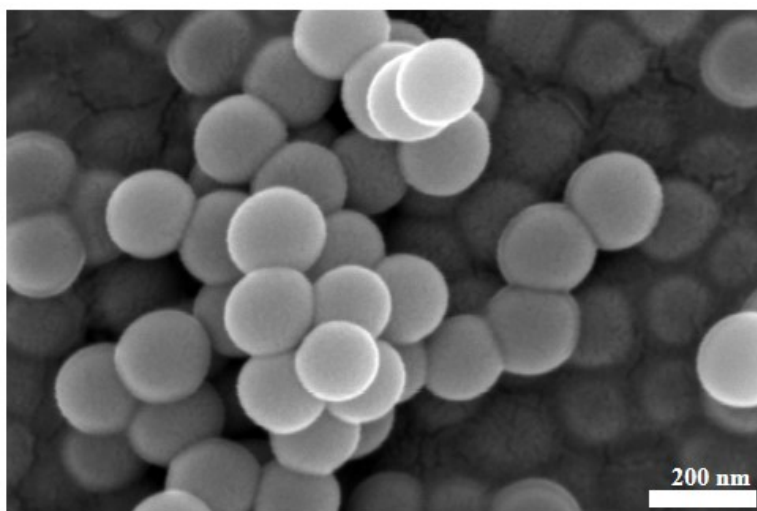
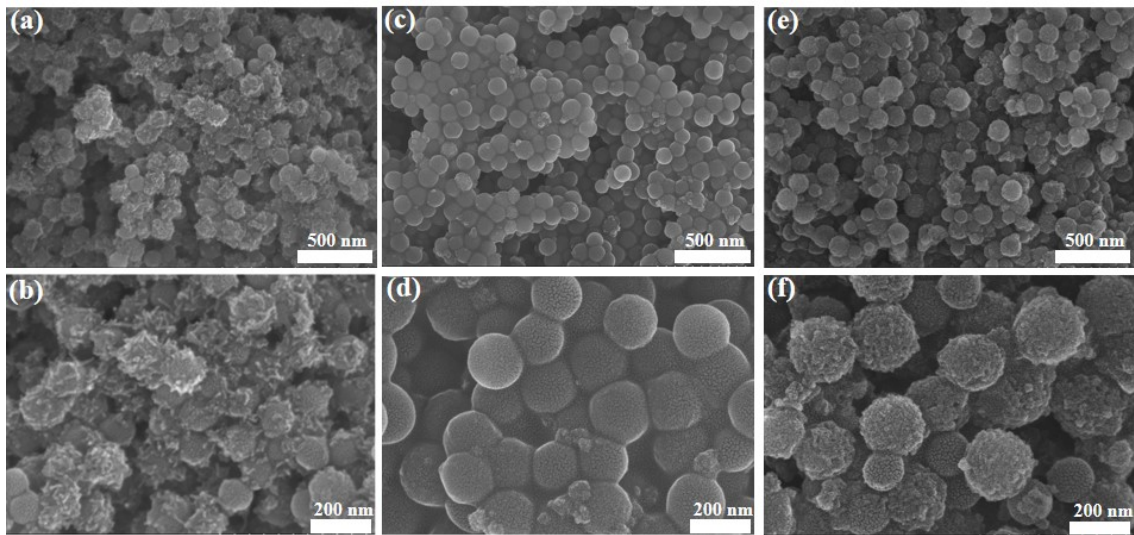
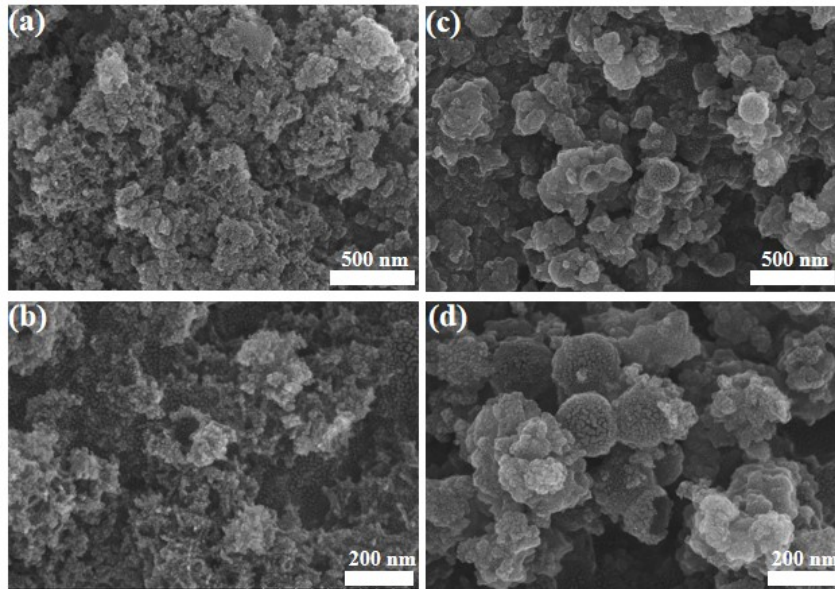


Figure S1. SEM image of  $\text{SiO}_2$ .



**Figure S2.** SEM image of  $\text{SiO}_2@\text{MnO}_2$  (a and b),  $\text{SiO}_2@\text{Fe}_3\text{O}_4@\text{C}$  (c and d), and  $\text{SiO}_2@\text{Fe}_3\text{O}_4@\text{MnO}_2$  (e and f).



**Figure S3.** SEM image of  $\text{MnO}_2\text{-HNS}$  (a and b), and  $\text{Fe}_3\text{O}_4@\text{C-HNS}$  (c and d).

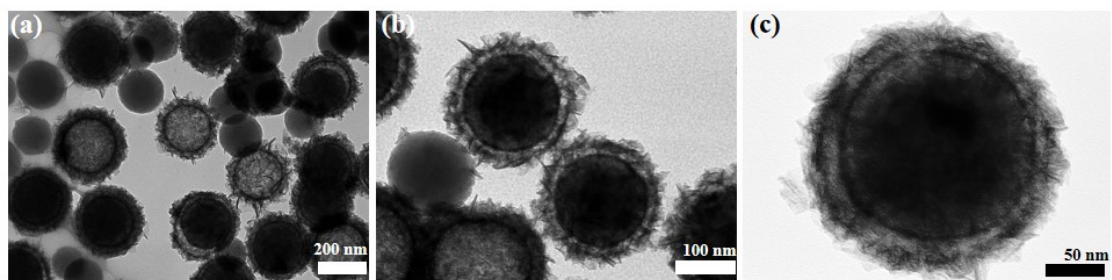


**Figure S4.** TEM image at different magnifications of  $\text{SiO}_2@Fe_3O_4@MnO_2$ (a-c).

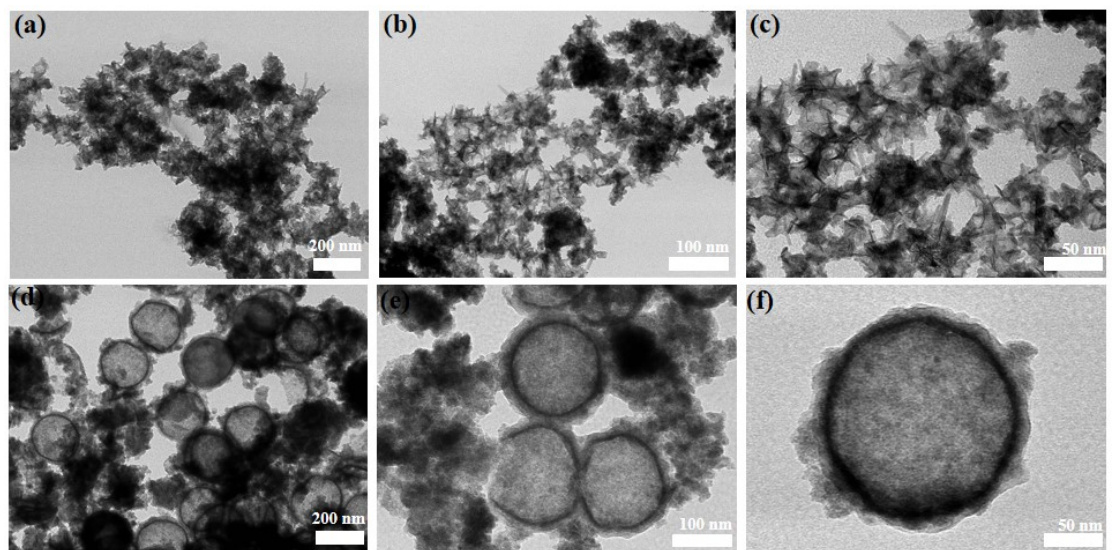


**Figure S5.** TEM image at different magnifications of (a-c) $MnO_2$ -HNS, and (d-f)  $Fe_3O_4@C$ -HNS.

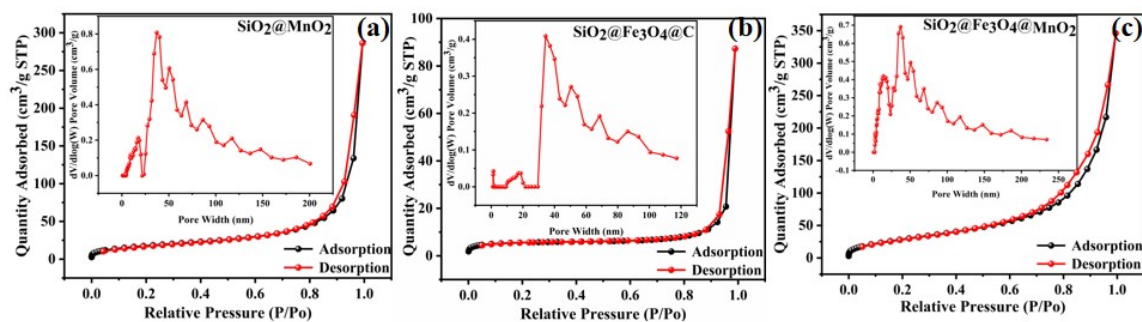


**Figure S6.** The nitrogen adsorption-desorption isotherms and the corresponding pore size distribution (inset) of (a) SiO<sub>2</sub>@MnO<sub>2</sub>, (b) SiO<sub>2</sub>@Fe<sub>3</sub>O<sub>4</sub>@C, and (c) SiO<sub>2</sub>@Fe<sub>3</sub>O<sub>4</sub>@MnO<sub>2</sub>.

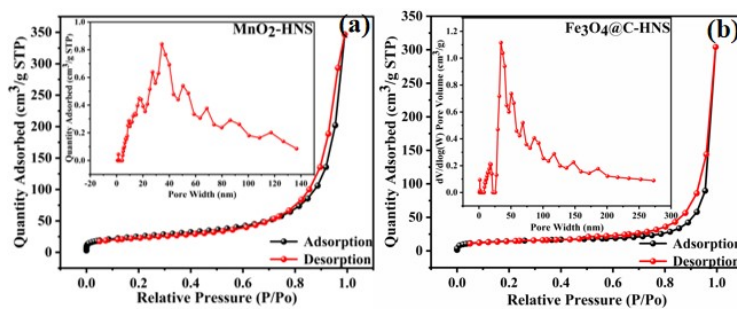


**Figure S7.** The nitrogen adsorption-desorption isotherms and the corresponding pore size distribution (inset) of (a) MnO<sub>2</sub>-HNS, and (b) Fe<sub>3</sub>O<sub>4</sub>@C-HNS.



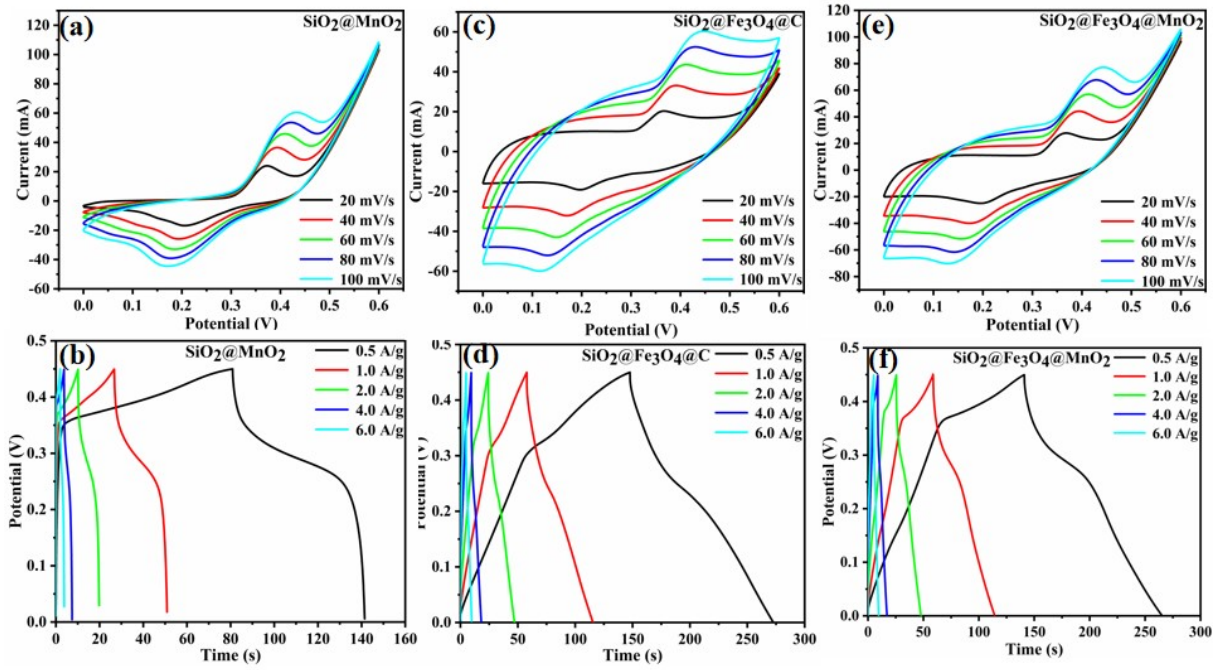


**Figure S8.** CV curves (a, c and e) and GCD (b, d and f) curves of (a and b)  $\text{SiO}_2@\text{MnO}_2$ , (c and d)  $\text{SiO}_2@\text{Fe}_3\text{O}_4@\text{C}$ , and (e and f)  $\text{SiO}_2@\text{Fe}_3\text{O}_4@\text{MnO}_2$ .

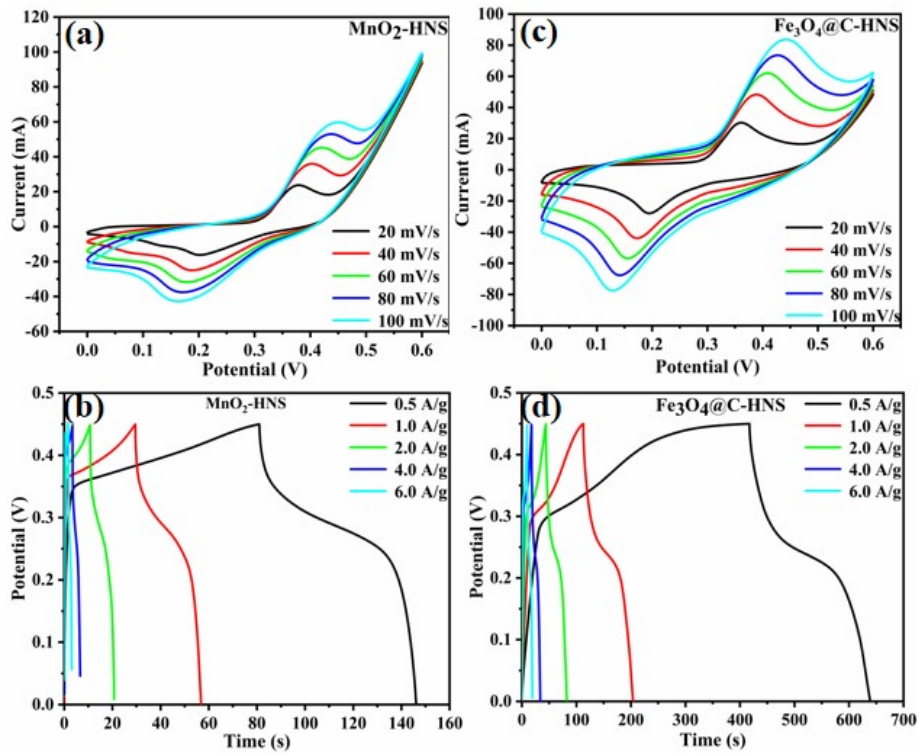


**Figure S9.** CV curves (a and c) and GCD (b and d) curves of (a and b)  $\text{MnO}_2\text{-HNS}$ , and (c and d)  $\text{Fe}_3\text{O}_4@\text{C-HNS}$ .

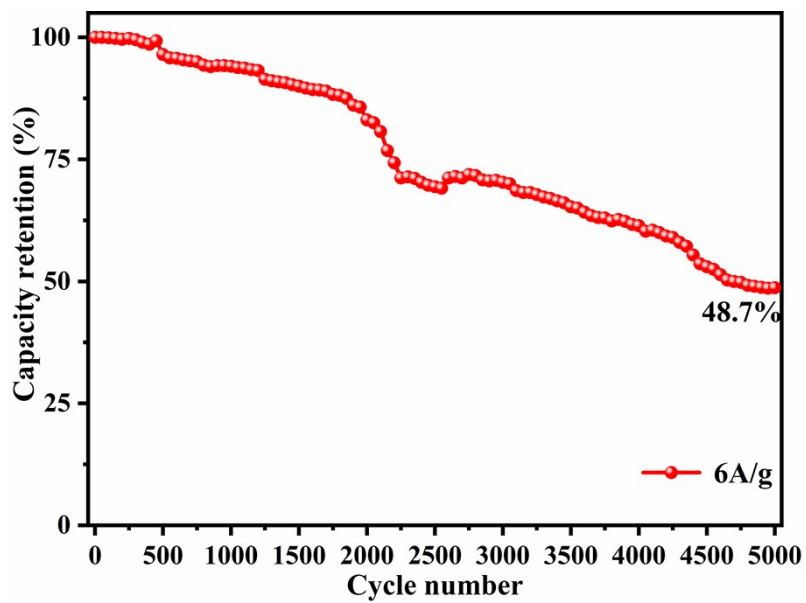


**Figure S10.** The cycling stability measured via the GCD experiments at 6 A g<sup>-1</sup> of Fe<sub>3</sub>O<sub>4</sub>@MnO<sub>2</sub>-HNS.

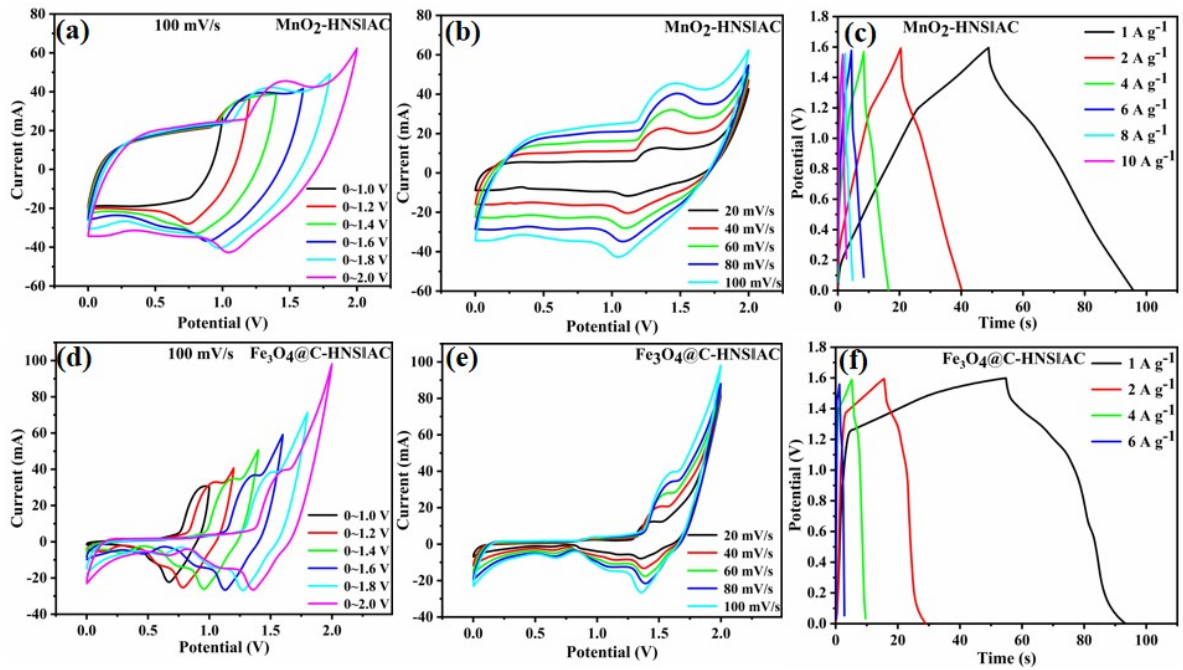


**Figure S11.** (a and d) CV curves at various potential windows at  $100 \text{ mV s}^{-1}$ , (b and e) CV curves at various scan rates, (c and f) GCD curves at various current densities of (a-c)  $\text{MnO}_2\text{-HNS}\|\text{AC}$ , and (d-f)  $\text{Fe}_3\text{O}_4\text{@C-HNS}\|\text{AC}$ .